Structural, Electronic, and Electrochemical Properties of Cathode Materials Li2MSiO4 (M = Mn, Fe, and Co): Density Functional Calculations

ARTICLE *in* THE JOURNAL OF PHYSICAL CHEMISTRY C · FEBRUARY 2010

Impact Factor: 4.77 · DOI: 10.1021/jp910746k

6 AUTHORS, INCLUDING:

Guohua Zhong
Shenzhen, Chinese Academy of Sciences
57 PUBLICATIONS **241** CITATIONS
SEE PROFILE

Yanling Li
Jiangsu Normal University
44 PUBLICATIONS **326** CITATIONS
SEE PROFILE

Structural, Electronic, and Electrochemical Properties of Cathode Materials Li_2MSiO_4 (M = Mn, Fe, and Co): Density Functional Calculations

Guohua Zhong,[†] Yanling Li,[‡] Peng Yan,[§] Zhuang Liu,[†] Maohai Xie,[||] and Haiqing Lin*,[†]

Center for Photovoltaics Solar Cell, Shenzhen Institutes of Advance Integration Technology, Chinese Academy of Sciences, Shenzhen, 518055, People's Republic of China, Department of Physics, Xuzhou Normal University, Xuzhou, 221116, People's Republic of China, Department of Physics, Binzhou Medical University, Yantai, 264003, People's Republic of China, and Department of Physics, The University of Hong Kong, Pokfulam Road, Hong Kong, People's Republic of China

Received: November 11, 2009; Revised Manuscript Received: January 18, 2010

For Li_2FeSiO_4, its $P2_1$ space group makes it possibly perfect as a new cathode material for Li-ion batteries (Nishimura et al. *J. Am. Chem. Soc.* **2008**, *130*, 13212). For this type of Li_2MSiO_4 (M = Mn, Fe, and Co), the structural, electronic, and electrochemical properties have been investigated, using the density functional theory with the exchange-correlation energy treated as the generalized gradient approximation (GGA) plus on-site Coulomb energy correction ($+U$). Within the GGA$+U$ framework, the fully lithiated Li_2MSiO_4 as well as the delithiated $LiMSiO_4$ and $MSiO_4$ are all semiconducting, and the band gap lowers with the extraction of lithium ions. The fully lithiated compounds are all stabilized at their ferromagnetic phase, while the delithiated compounds are all stabilized when antiferromagnetic. Starting from the $P2_1$ structure, the fully delithiated $MSiO_4$ has better stability than that obtained from $Pmn2_1$ structure. In Li_2FeSiO_4, the possibility of reversibly extracting more than one lithium ion is enhanced because of the lower stability of the intermediate phase $LiFeSiO_4$ comparing with the $Pmn2_1$ symmetry situation. Li_2MnSiO_4 with the $P2_1$ symmetry has higher electronic conductivity, and Li_2CoSiO_4 has the suitable second-step voltage of less than 5.0 V. All Li_2FeSiO_4, Li_2MnSiO_4, and Li_2CoSiO_4 are predicted as promising cathode materials.

Introduction

Li_2MSiO_4 (M denotes transition metals) has attracted considerable attention ever since Li_2FeSiO_4 was synthesized and characterized by Nytén et al.[1] Numerous experimental research[1−13] and theoretical calculations[14−19] have been done to find cheaper cathode materials for Li-ion batteries with higher intrinsic capacity and better electronic conductivity than the currently popular $LiFePO_4$. With regard to the crystal structure of Li_2FeSiO_4, Nytén et al. suggested an orthorhombic β-Li_3PO_4-based structure with the $Pmn2_1$ symmetry. In this proposed structure, all the cations occupy half of the tetrahedral sites in a slightly distorted *hcp* oxygen array, forming a corner-sharing network of tetrahedra (trigonal pyramid) with an identical upward direction. Under this structural model, Li_2FeSiO_4 has high electronic conductivity, but the theoretical capacity is somewhat low and the reversibility and the cycling performance are not good.[15] The isomorphic Li_2MnSiO_4 has a high theoretical capacity and stability, but it has poor electronic conductivity.[4,9,15] It was theoretically predicted that the lithium extraction voltage of Li_2CoSiO_4 is too high for current electrolytes,[15] though recent research has indicated that the $Pmn2_1$ symmetrical Li_2CoSiO_4 material is a potential candidate for the high-capacity cathode of advanced lithium ion batteries.[8,9,16] However, many reports[4,8,9,13] have indicated that the series of Li_2MSiO_4 compounds might be used as potentially cheap cathode materials for advanced rechargeable lithium ion batteries. It is key point how to improve these materials.

In a very recent report on Li_2FeSiO_4, Nishimura et al.[13] proposed a different structure model with the $P2_1$ symmetry using high-resolution synchrotron XRD and transmission electron microscope technologies. Unlike Nytén's model, the FeO_4/SiO_4 trigonal pyramids periodically take opposite orientations in Nishimura's model. The $P2_1$ symmetrical Li_2FeSiO_4 is regarded as a perfect cathode material. But the study of the stability, electronic properties, and electrochemical performance of this $P2_1$ symmetrical compounds is still an open question, with a comparison of that the theoretical calculations[14−19] on $Pmn2_1$ symmetrical Li_2MSiO_4 have been reported extensively. To understand the advantage as well as the disadvantage, we have investigated the $P2_1$ symmetrical Li_2MSiO_4 (M = Mn, Fe, and Co) within the first-principles framework, because the first-principles calculation has been widely used to search for promising electrode materials in the past decade. The paper is structured as follows. In the second section, we present the Computational Details. In Results and Discussion, we analyze and discuss the calculated results in detail, including the structural stabilities, bonding characters (Structural Stabilities and Bonding Characters), electronic properties of fully lithiated Li_2MSiO_4 (Electronic Properties of Li_2MSiO_4), electronic properties of delithiated $LiMSiO_4$ and $MSiO_4$ (Electronic Properties of $LiMSiO_4$ and $MSiO_4$), and calculated average voltages (Average Deintercalation Voltages), respectively. Finally, fourth section is devoted to Conclusions.

Computational Details

Starting from the experimental lattice parameters and atomic positions,[13] the full optimization was first performed by the

* To whom correspondence should be addressed. Phone: +852 2609 6365. Fax: +852 2603 5204. E-mail: hqlin@phy.cuhk.edu.hk.
[†] Shenzhen Institutes of Advance Integration Technology
[‡] Xuzhou Normal University
[§] Binzhou Medical University
[||] The University of Hong Kong

10.1021/jp910746k
Published on Web 02/05/2010

TABLE 1: Optimized Lattice Parameters and Unit Cell Volume (Å^3) of Li_2MSiO_4, $LiMSiO_4$, and $MSiO_4$ (M = Mn, Fe, and Co) Compared with Available Experimental Results

compounds	a (Å)	b (Å)	c (Å)	α (°)	β (°)	γ (°)	V (Å ^{3})
Li_2MnSiO_4	8.30936	5.08860	8.33527	89.62	97.91	90.76	349.05
$LiMnSiO_4$	9.04543	5.42721	7.34782	90.08	97.54	90.07	353.60
$MnSiO_4$	7.05598	5.04034	9.06175	100.18	101.33	101.02	302.39
Li_2FeSiO_4	8.22783	5.09290	8.25958	89.63	98.70	90.68	342.09
	8.22898[a]	5.02002[a]	8.23335[a]		99.2027[a]		335.74[a]
$LiFeSiO_4$	8.70468	5.28822	7.85377	90.00	94.26	90.00	360.53
$FeSiO_4$	7.13308	5.25874	9.08786	102.39	99.14	104.05	314.87
Li_2CoSiO_4	8.18588	5.05985	8.23085	89.70	96.68	90.59	338.58
$LiCoSiO_4$	8.55194	5.26732	7.93282	90.01	94.57	90.03	356.21
$CoSiO_4$	7.06521	5.39744	9.10560	100.17	102.40	101.52	301.96

[a] Ref 13.

Vienna ab initio Simulation Package (VASP)[20,21] within the projector augmented wave (PAW) approach.[22] A 500 eV cutoff for the plane-wave basis set was used. The convergence thresholds were set as 10^{-5} eV in energy and 0.01 eV/Å in force. From the optimized structures, the structural stability and bonding character were analyzed.

To calculate self-consistent properties such as charge density, density of states, and magnetism, we employed the highly precise full-potential linearized augmented plane wave (FLAPW) method,[23,24] which treats all electrons and has no shape approximations for the potential and the charge density, as implemented in the WIEN2k simulation package.[25] Within the FLAPW method, the unit cell is divided into nonoverlapping muffin-tin (MT) spheres and an interstitial region. Inside the muffin-tin sphere of radius R_{MT}, the wave functions are expanded using radial functions (solution to the radial Schröinger equation) times spherical harmonics up to l_{max}^{wf}, and the expansion of the potential inside the muffin-tin spheres is carried out up to l_{max}^{pot}. The parameter $R_{MT}^{min} \times K_{MAX}$ (R_{MT}^{min} is the smallest muffin-tin spherical radius present in the system and K_{MAX} is the truncation of the modulus of the reciprocal lattice vector) is used to determine the number of plane waves needed for the expansion of the wave function in the interstitial region, while the parameter G_{MAX} is used to truncate the plane-wave expansion of the potential and density in the interstitial region. Here, the MT radii were set to 1.6, 1.9, 1.6, and 1.2 au for the Li, M (Mn, Fe, and Co), Si, and O atoms, respectively. And, we let $R_{MT}^{min} \times K_{MAX} = 7.0$, $l_{max}^{wf} = 10$, $l_{max}^{pot} = 4$, and $G_{MAX} = 12$. The separate energy of −8.0 Ry was used between valence and core states. Integrations in the first Brillouin zone (FBZ) have been performed using the 2 × 4 × 2 Monkhorst-Pack special k-points.[26] Self-consistency calculation of electronic structures was achieved when the total-energy variation from iteration to iteration converged to a 0.01 mRy accuracy or better.

The exchange-correlation energies for both VASP-PAW and WIEN2k-FLAPW were treated as the generalized gradient approximation (GGA) of Perdew-Burke-Ernzerhof (PBE) version.[27] Furthermore, to deal with the 3d electron−electron correlation, GGA+U type calculation[28] was carried out with the on-site Coulomb energy (U) and exchange interactions (J) treated by a single effective parameter $U' = U - J$.[29] Generally two ways are followed to estimate U'. First, U' can be directly calculated by using the constrained local density approximation (LDA) method. However, it is not so meaningful to take this approach in the plane-wave method because of some arbitrariness in the definition of localized orbitals. The second way is to adjust U' so as to fit the calculated band gap with an experimental one. It is well-known that density functional theory is bad at calculating band gaps, especially for transition metal oxides. So the LDA(GGA)+U method was proposed to reproduce band gaps by adjusting parameter U'. Here, we used $U' = 5.0$ eV for M = Mn, Fe, and Co compounds to reproduce experimental band gaps. Such a parameter has been checked as a suitable parameter by previous related research.[15,17,30,31]

Results and Discussion

Structural Stabilities and Bonding Characters. To obtain the stable configuration, we carried out the full optimization calculations for Mn, Fe, and Co compounds within the VASP package based on the PAW method. The optimized lattice constants, angles, and equilibrium volumes are listed in Table 1. All relaxed internal coordinates are summarized in Supporting Information (SI). For Li_2FeSiO_4, the calculated crystal parameters are in good agreement with the available experimental data,[13] which implies the reliability of the GGA+U type treatment. The cell volumes of Li_2MnSiO_4 and Li_2CoSiO_4 are slightly larger and less than that of Li_2FeSiO_4, respectively. However, Fe, Mn, and Co compounds have the identical symmetry. So Figure 1 shows optimized geometrical structures in the case of Fe compound. Differing from the $Pmn2_1$ symmetrical structure,[1] the $P2_1$ symmetrical Li_2MSiO_4 is a monoclinic structure with the increase of a and c lattice constants, as shown in Table 1 and Figure 1a. MO_4 and SiO_4 trigonal pyramids link along[10] direction and periodically take

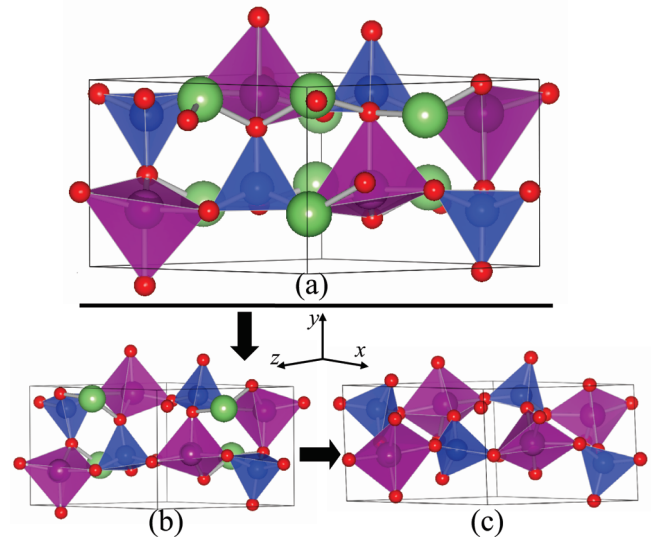

Figure 1. Optimized crystal structure: (a) Li_2MSiO_4; (b) $LiMSiO_4$; and (c) $MSiO_4$ (M = Mn, Fe, and Co). Green and red balls correspond to Li and O atoms, and M−O and Si−O polyhedra are shown by purple and blue trigonal pyramids, respectively.

opposite orientations in this structure with M and Si atoms located in the central sites of the oxygen tetrahedra. Each SiO_4 tetrahedron shares its four corners with four neighboring MO_4 tetrahedra and vice versa. There are four Li_2MSiO_4 formula units (f.u.) per unit cell, that is, each unit cell contains 8 lithium, 4 M, 4 silicon, and 16 oxygen atoms. Li_2MSiO_4 with the $P2_1$ symmetry is a obvious layered material. Comparing the relative stability of Li_2MSiO_4 with various symmetries from the calculated total energies, we found that the $P2_1$ symmetry results in higher energies of 0.073, 0.021, and 0.031 eV/f.u. for Mn, Fe, and Co compounds than the $Pmn2_1$ symmetry. The lower stability of $P2_1$ symmetry indicates that the possibility of reversibly extracting of more than one lithium ion in Li_2MSiO_4 increases.

The initial crystal structures of delithiated compounds $LiMSiO_4$ and $MSiO_4$ (M = Mn, Fe, and Co) were obtained by removing Li atoms from the corresponding Li_2MSiO_4 unit cells, then the crystallographic cell parameters (the cell shape as well as the lattice constants) and the internal coordinates were relaxed (see SI). The obtained structures could not be guaranteed to be the ground-state ones because they were only relaxed from the initial monoclinic configuration. Hence, the different Li arrangements were considered during the optimization calculations to seek more stable state of $LiMSiO_4$. Figure 1b shows the stable $LiMSiO_4$ structure and the optimized parameters are listed in Table 1 and Table S2 of SI, respectively. Removing half of Li atoms from Li_2MSiO_4, the lattice constants increase along a and b directions while decreases along the c direction, which results in the larger cell volume than corresponding fully lithiated compounds. The phenomenon of unusual variation of cell volume was also observed in $Pmn2_1$ symmetrical Li_2MSiO_4.[14,16,17,19] The ionic valent state changes from M^{2+} to M^{3+} in $LiMSiO_4$, but this does not induce the variation of coordination number of M ion. A large number of vacancies are produced and become ordering (namely, defect association) after extracting Li atoms. It is possibly the reason of unusual variation of cell volume. However, the issue is still open with leaving for future study. Here, the expanding extent of cell volume of $LiMSiO_4$ relative to Li_2MSiO_4 is stronger than the $Pmn2_1$ symmetrical materials. It is an implication of the stability lowering of the intermediate phase $LiMSiO_4$. The slight distortion of $M-O$ and $Si-O$ tetrahedra makes the arrangement of MO_4 and SiO_4 trigonal pyramids become irregular in $LiMSiO_4$. But the angles of α and γ are still close to 90°. $LiMSiO_4$ remains the $P2_1$ symmetry.

Following the reaction

$$\frac{1}{2}Li_2MSiO_4 + \frac{1}{2}MSiO_4 \leftrightarrow \lim SiO_4 \qquad (1)$$

to analyze the stability of intermediate phase $LiMSiO_4$, the formation energies of $LiMSiO_4$ was calculated from the total energy expression,

$$E_f = E[\lim SiO_4] - \frac{1}{2}E[Li_2MSiO_4] - \frac{1}{2}E[MSiO_4] \qquad (2)$$

Figure 2 shows the formation energy dependence on transition metals in $LiMSiO_4$. The formation energies of $LiMnSiO_4$, $LiFeSiO_4$, and $LiCoSiO_4$ are −0.099, −0.681, and −0.367 eV/f.u., respectively. The negative energy indicates that $LiMSiO_4$ is stable with respect to phase separation into Li_2MSiO_4 and $MSiO_4$ at low temperatures. Comparing with the formation

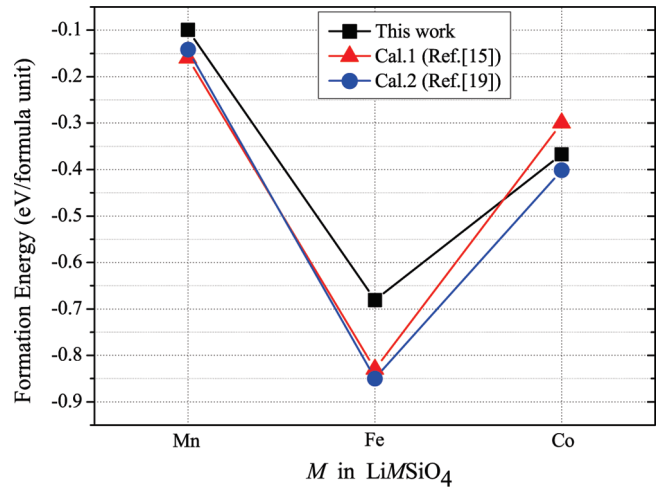

Figure 2. Calculated formation energies of the intermediate phase $LiMSiO_4$ compared with the previous calculations (refs 15 and 19), in units of eV per formula unit.

energy obtained from the $Pmn2_1$ structure,[15,19] the absolute values of formation energy of $LiMSiO_4$ decreases, which may be explained from the cell volume variation of $LiMSiO_4$ obtained from $P2_1$ symmetry being stronger than that obtained from $Pmn2_1$ symmetry, as discussed above. Consequently, the stability of the intermediate phase $LiMSiO_4$ decreases and the reversibility and the cycling performance are improved. However, for the same type of symmetry, the absolute values of formation energies show that $LiMnSi_4$ has the low stability, while $LiFeSiO_4$ has the slightly high stability. $LiMnSiO_4$ has better reversibility and cycling performance than $LiCoSiO_4$ and $LiFeSiO_4$.

Removing all Li atoms, the crystal parameters (see Table 1 and SI) were visibly varied, and the cell volume of $MSiO_4$ is the smallest among these three lithium concentrations, which is different from the previous studies on the $Pmn2_1$ structural situation.[14,16,17,19] From the $Pmn2_1$ structure, the extraction of Li atoms makes $MSiO_4$ expand. On the contrary, the $MSiO_4$ is compressed after extracting Li atoms in our study, which is the expected result. The condensation of cell volume indicates that the stability of $MSiO_4$ is increased. It is important to experimentally obtain the stable $MSiO_4$ sample because researchers have difficulty in obtaining $MSiO_4$ from $Pmn2_1$ symmetrical structures. The calculated total energies show that the $MSiO_4$ obtained from $P2_1$ symmetry is more stable than that from $Pmn2_1$ symmetry, with the total energies lowering 0.472, 0.290, and 0.064 eV/f.u. for Mn, Fe, and Co systems, respectively. Comparing the coordination number of the M ion, in addition, it transforms to five in $MSiO_4$ from four in Li_2MSiO_4 and $LiMSiO_4$, which was not presented in previous reports.[14,16,17,19] Removing all Li atoms, more vacancies are produced, which destroy the vacancy ordering and result in the crystal collapse, comparing with $LiMSiO_4$. After reconstruction of the $M-O$ polyhedra, compression of the system and the variation of the coordination number in $MSiO_4$ are found. Structural transformation from $LiMSiO_4$ to $MSiO_4$ is obvious. Furthermore, the arrangements of MO_5 polyhedra and SiO_4 trigonal pyramids are more disordering. This distortion increases the stability of $MSiO_4$.

To investigate the detailed variation in structures, we have examined the interatomic distances. Figure 3 shows the variations of $M-O$ and $Si-O$ bond lengths in $Li_x MSiO_4$ (x = 2, 1, and 0). The vertical bar indicates the spread between maximum and minimum bond lengths in unit cell, and short horizontal bar represents the average value of bond lengths. It is noticeable

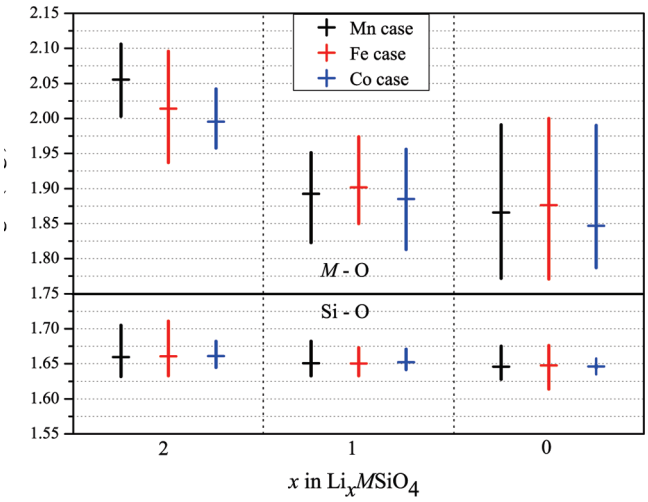

Figure 3. Averaged bond lengths (short horizontal bars) of $M-O$ (the upper panels) and Si−O (the lower panels) dependence on different lithium concentrations $x = 2$, 1, and 0 in Li$_x$ MSiO$_4$. The vertical bar indicates the spread between the maximum and the minimum bond lengths in the unit cell.

that the bond lengths of $M-O$ are much longer than those of Si−O, which means that the bonding character of $M-O$ is different from that of Si−O. From Li$_2M$SiO$_4$ to LiMSiO$_4$ and to MSiO$_4$, the transition metal is oxidized from M^{2+} to M^{3+} and M^{4+} valence states. The calculated average bond lengths of $M-O$ monotonously decrease due to the so-called rehybridization shift,[31] which occurs in the transition metal ligand bond at high levels of oxidation in order to diminish the effect of changing the valence on the transition metal site. However, the average bond lengths of Si−O are almost unchanged, which means that the bonding nature between Si and O atoms remains unchanged during the lithiation−delithiation process. The structural stability of Li$_2M$SiO$_4$ during lithium deintercalation is actually the consequence of a strong covalent Si−O bond. For the same lithium concentration, the order of average bond lengths in Li$_2M$SiO$_4$ is $L_{Mn-O} > L_{Fe-O} > L_{Co-O}$, which is explained by the M ionic radii $r_{Mn^{2+}} > r_{Fe^{2+}} > r_{Co^{2+}}$.[32] In nonstoichiometric LiMSiO$_4$ and MSiO$_4$, the oxide state of the M ion is complicated, and the ionic radii order has the change of $r_{Fe^{3+}} > r_{Mn^{3+}} > r_{Co^{3+}}$, as well as for M^{4+} valence state. So the orders of average bond lengths are both $L_{Fe-O} > L_{Mn-O} > L_{Co-O}$ in LiMSiO$_4$ and MSiO$_4$. From the spread between maximum and minimum bond lengths in the unit cell, it is established that the distortion of the $M-O$ polyhedra in MSiO$_4$ is the biggest. As a comparison, our calculated bond lengths are in agreement with experiment.[13] Comparing with the bond length results from the $Pmn2_1$ space group,[19] our calculated $M-O$ bond lengths are correspondingly shorter than those in the $Pmn2_1$ structure at $x = 2$. The average bond lengths of Fe−O and Co−O are very close to the previously calculated results at $x = 1$, while they are a little larger than previously calculated results at $x = 0$. And the average bond lengths of Mn−O are correspondingly less than those in the $Pmn2_1$ structure at $x = 1$ and 0.

The different charge densities, defined as the difference between the crystalline electron density and the superposition of electron densities from the neutral atoms, is helpful for visualizing the bonding characteristics. Figure 4 shows the 3D plots of different charge density for the Fe case, containing Fe−O and Si−O bonding pictures. It is clear that the covalent bonding character is observed between Si and O atoms due to the charge density accumulation between them. The sp^3

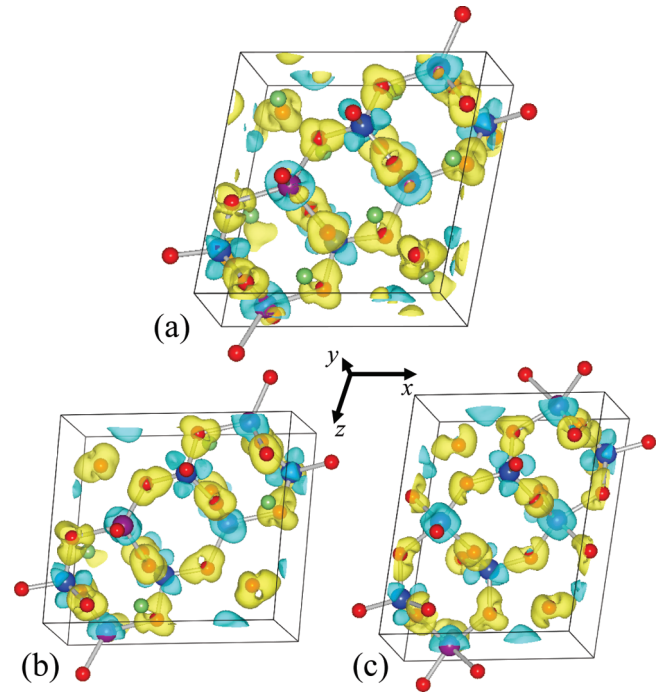

Figure 4. 3D plots of different charge densities for Fe compounds, the isovalue is 0.02. The positive and negative densities are in yellow and blue, respectively. (a) Li$_2$FeSiO$_4$, (b) LiFeSiO$_4$, and (c) FeSiO$_4$.

hybridization exists between Si and O atoms, forming the σ bonds. The stability of the system is induced by these stable σ bonds. The interaction between Fe and O atoms comes from the hybridization of $3d$ and $2p$ orbits with the π-bonding character. However, the phenomena of the charge density depletion around the Fe atom and the charge density accumulation around O atoms are also clearly visible in these plots. Charge transfer from Fe to O atoms implies that the Fe−O bonding has much more ionic feature. From Li$_2$FeSiO$_4$ to LiFeSiO$_4$ and FeSiO$_4$, the charge transfer phenomenon between Fe and O atoms becomes more significant, while the covalent bonding feature between Si and O atoms is almost unchanged. Like the Fe compound, similar bonding phenomena are observed in Mn and Co cases.

Electronic Properties of Li$_2M$SiO$_4$. The calculated magnetic energies ΔE_m, defined as the difference of total energies for ferromagnetic (FM) and antiferromagnetic (AFM) states: $E_{FM} - E_{AFM}$, are listed in Table 2. The negative values of magnetic energies (−2.793, −2.653, and −2.594 eV/f.u.) indicate Li$_2M$SiO$_4$ is stabilized at the FM ground state, which is different from the $Pmn2_1$ structure stabilized at the AFM ground state.[6,33] The different magnetism results possibly arise from the difference in crystal structures. The spin-polarized density of states (DOS) of Li$_2M$SiO$_4$ are shown in Figure 5. The projected DOS onto the d orbit of the M atom and the p orbit of the O atom are presented within GGA and GGA+U framework, respectively. As shown in Figure 5, the electronic structures predicted by the GGA+U method can be quite different from that predicted by the GGA. The Coulomb energy U results in the increase in spin-splitting, that is, pushing the majority-spin and minority-spin states toward lower and higher energy levels, respectively. Obviously, more accurate treatment of the Coulomb correlations through the GGA+U method yields the band gap fitting with experiment. Table 2 also summarizes the calculated band gaps of all systems and average magnetic moments per M ion, comparing with previous results obtained from $Pmn2_1$ structure. For Li$_2$MnSiO$_4$, the band gap changes to 3.44 eV from

TABLE 2: Calculated Magnetic Energy per Formula Unit (ΔE_m), Band Gap (E_g), and Average Magnetic Moment (m) per M Ion in $Li_x MSiO_4$ (M = Mn, Fe, and Co)

	Mn			Fe			Co		
	$x = 2$	$x = 1$	$x = 0$	$x = 2$	$x = 1$	$x = 0$	$x = 2$	$x = 1$	$x = 0$
ΔE_m (eV)	−2.793	0.043	0.055	−2.653	0.051	0.001	−2.594	0.062	0.133
E_g (eV)	3.44	1.74	0.83	2.75	2.67	0.10	3.75	1.80	0.41
	4.25[a]	0.9[a]		3.0[a]	2.38[a]		4.07[a]	1.4[a]	
	3.4[b]	0.5[b]	metal[b]	3.3[b]	2.4[b]	metal[b]	3.7[b]	1.9[b]	1.0[b]
m (μ_B)	4.28	3.58	2.90	3.51	4.12	3.65	2.64	3.11	3.33
	4.70[b]	4.10[b]	3.94[b]	3.76[b]	4.29[b]	4.11[b]	2.80[b]	3.20[b]	3.35[b]

[a] Ref 15. [b] Ref 19.

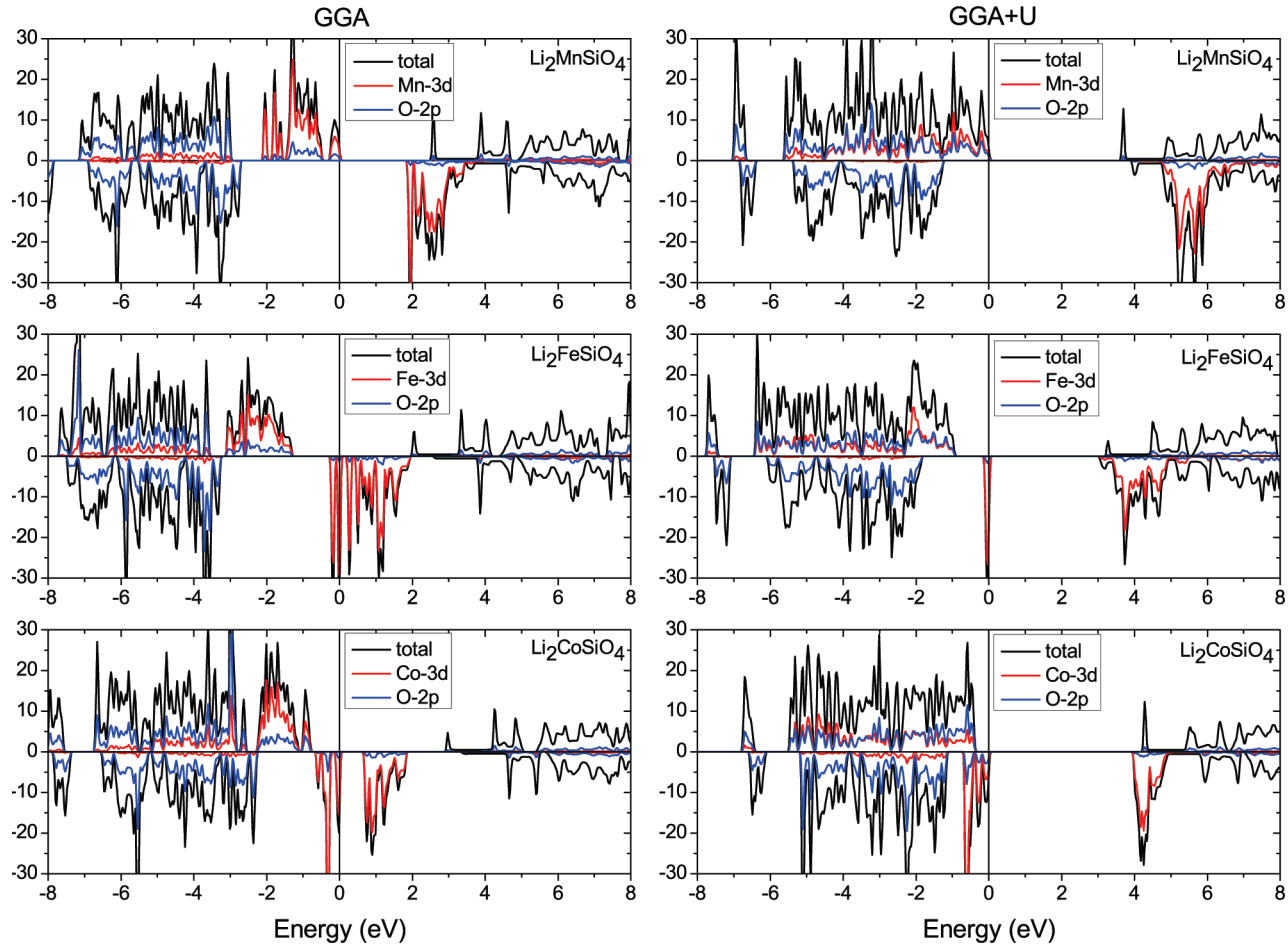

Figure 5. Total and projected density of states in Li_2MSiO_4 (M = Mn, Fe, and Co) calculated by the normal GGA (left panels) and the GGA+U methods (right panels).

1.8 eV with plus U. The band gap of Li_2CoSiO_4 is 3.75 eV predicted by the GGA+U instead of 0.6 eV predicted by the GGA. Especially the transition from metal to insulator occurs in Li_2FeSiO_4, with a band gap of 2.75 eV. For the $Pmn2_1$ structure, although the calculations were treated with the GGA+U method, the calculated band gap has a big difference,[15,19] shown in Table 2. Comparing with the calculated results of the $Pmn2_1$ structure, our calculated band gaps are close to the values reported by Wu et al.[19] However, our obtained band gap of Mn and Co compounds is visibly less than the reported values (about 4.25 and 4.07 eV for Mn and Co cases, respectively) by Arroyo-de Dompablo et al.[15] Hence, the $P2_1$ structure can generally result in a lower band gap than $Pmn2_1$ case. The monoclinic structure has lower band gap than the orthorhombic one that has also been established by the previous report of Li_2MnSiO_4.[17] From the electronic structures obtained by the GGA, in addition, the visible 3d band splitting is observed in majority-spin channel, forming two or more valence bands. Plus U, the band splitting disappears, and 3d bands are more dispersive. There is stronger hybridization between M-3d and O-2p electronic states in the range of −6∼0 eV. On the contrary, the minority-spin 3d states are always localized in Li_2MSiO_4.

In spite of the almost same crystal structure, Mn, Fe, and Co compounds show the different electronic structures, which arises from different electronic configurations of $3d^5 4s^2$ in Mn, $3d^6 4s^2$ in Fe, and $3d^7 4s^2$ in Co atom. In Li_2MSiO_4, the transition metals exhibit M^{2+} valence state with electronic configurations of $3d^5$, $3d^6$, and $3d^7$ for Mn^{2+}, Fe^{2+}, and Co^{2+} ions, respectively. As the DOS plot shown in Figure 5, the majority-spin states of Mn-3d are fully occupied, while the minority-spin states are fully empty. This means that 3d electrons are all spin-up for Mn^{2+}, in high-spin state with $S \sim (5/2)$. For Li_2FeSiO_4, a very sharp DOS peak is below the Fermi level in spin-down channel, which indicates that a little minority-spin state are also occupied

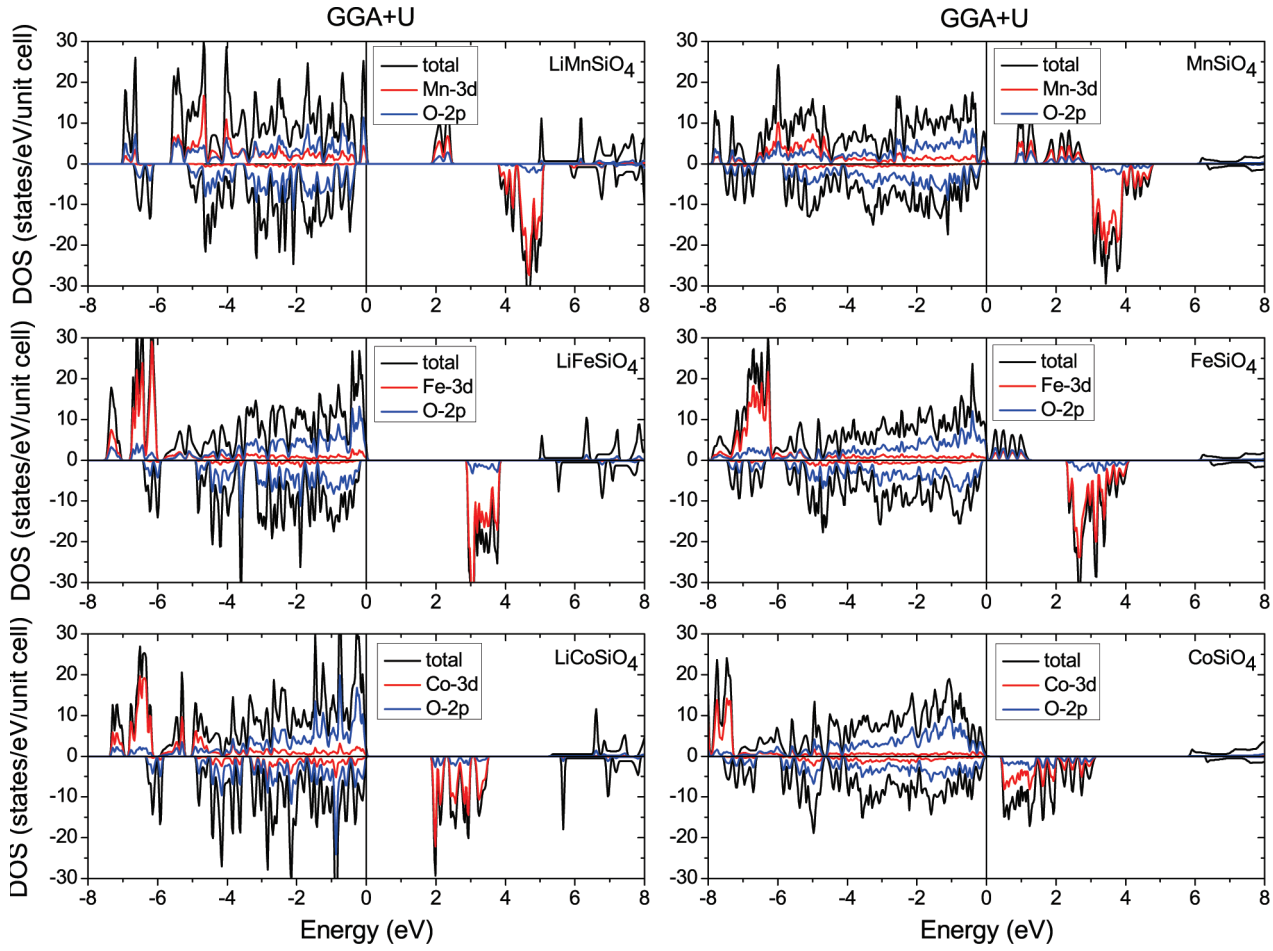

Figure 6. Total and projected density of states in LiMSiO$_4$ (left panels) and MSiO$_4$ (right panels) calculated by the GGA+U method.

besides majority-spin states. From the refine projected DOS, we find the occupancy less than one electron in the spin-down t_{2g} states. And Fe^{2+} ions are also in high-spin state with $S \sim 2$. For Li_2CoSiO_4, shown in Figure 5, three DOS peaks are below the Fermi level with more 3d electrons occupying the spin-down t_{2g} orbital than Fe^{2+} ion. And the majority-spin states are also fully occupied. Hence, Co^{2+} ions are in high-spin state with $S \sim (3/2)$. Under the crystal fields, the calculated spin magnetic moments per Mn^{2+}, Fe^{2+}, and Co^{2+} are 4.28, 3.51, and 2.64 μ_B, which are correspondingly less than those in isolated ions. And there is a big difference from the $Pmn2_1$ structures calculated by the pseudopotential method.[19]

Electronic Properties of LiM SiO$_4$ and M SiO$_4$. The positive magnetic energy values shown in Table 2 indicate that both LiMSiO$_4$ and MSiO$_4$ stabilize at the AFM phases. However, the total energy difference between FM and AFM phases is small, especially for FeSiO$_4$, that is, ~1 meV/f.u.. Therefore, the use of FM data for LiMSiO$_4$ and MSiO$_4$ does not affect our qualitative analysis. Figure 6 presents the FM spin-polarized DOS of LiMSiO$_4$ (left panels) and MSiO$_4$ (right panels). In the spin-up channel of LiMnSiO$_4$, there are some unoccupied Mn-3d states around 2 eV over the Fermi level, and the center of the Mn-3d bands shift toward lower energy level, compared with Li_2MnSiO_4. On the contrary, in the spin-down channel of LiFeSiO$_4$, the Fe-3d sharp-peak below the Fermi level disappears, which results in the fully empty minority-spin states in this system. The occupied 3d minority-spin states also decrease in LiCoSiO$_4$, compared with Li_2CoSiO_4. And the shift phenomenon of 3d bands center also occurs in LiFeSiO$_4$ and LiCoSiO$_4$. The variations of crystal structure from Li_2MSiO$_4$ to LiMSiO$_4$ result in the difference of the band split. It is clear that the valence state of transition metal ions occurs in a change from M^{2+} to M^{3+}, while the valence state of Si is almost invariable. The change of electronic configurations of M ions in LiMSiO$_4$ induces a smaller spin-split in valence bands and a bigger spin-split in conduct bands. From the projected DOS shown in Figure 6, the covalent hybridization between M-3d and O-2p becomes weak and the charge transfer between M and O enhances the ionic character in LiMSiO$_4$. From LiMSiO$_4$ to MSiO$_4$, the charge further transfers into O-2p orbits from M ions that exhibit the M^{4+} valence states. The ionic bonding character also exists between M and O atoms in MSiO$_4$, because there is a big charge transfer and a weak covalent hybridizing between the M and O atoms.

The calculated band gaps shown in Table 2 are 1.74, 2.67, and 1.80 eV for LiMnSiO$_4$, LiFeSiO$_4$, and LiCoSiO$_4$, respectively. Comparing with Li_2MSiO$_4$ systems, the band gaps of Mn and Co compounds is visibly decreased in LiMSiO$_4$, while that of Fe case is almost unchanged. It shows that the wave functions have stronger overlap in LiMnSiO$_4$ and LiCoSiO$_4$ than LiFeSiO$_4$, as the M−O bond length decreases (see Figure 3). For M^{3+} systems, electronic configurations transform to d^4 (Mn^{3+}), d^5 (Fe^{3+}), and d^6 (Co^{3+}). Calculated spin magnetic moments are, respectively, 3.58, 4.12, and 3.11 μ_B per M ion, which indicates that the M^{3+} is also in a high-spin state. In MSiO$_4$ systems, the band gap further decreases, 0.83, 0.10, and 0.41 eV for Mn, Fe, and Co cases. The band gap of Fe compound has a dramatic change. The obvious variation of band gap after extracting Li ions was also observed in $Pmn2_1$ symmetrical systems.[15,19] In M^{4+} ions, the electronic configura-

tions transform d^3 (Mn^{4+}), d^4 (Fe^{4+}), and d^5 (Co^{4+}). The calculated local spin magnetic moments are, respectively, 2.90, 3.65, and 3.33 μ_B, and M^{4+} are still in high-spin state.

Clearly, the change of band gap mainly induced by the variation of the interaction of $M-O$ atoms, because the interaction of Si−O atoms is almost unchanged with the variation of Li ionic concentration in systems. This type of material is not only the Mott-Hubbard insulator but also the charge transfer insulator from the shift of projected DOS shown in Figures 5 and 6. The lithiation−delithiation process leads to the structural variations as well as the variation of the interaction of M-O atoms. From Li_2MSiO_4 to $LiMSiO_4$ and to $MSiO_4$, the charge transfer from M to O ions makes the band gap decrease. Removing Li atoms, the metallic characteristic enhances with the increase of $M-O$ ionic bonding interaction so that the band gap becomes smaller. However, comparing the structures obtained from the $Pmn2_1$ symmetry, strong interaction still results in the big enough band splitting in fully delithiated $MSiO_4$, which is why the semiconductive behavior still exists in our investigations but metallic features partly suggested in the previous report of $MSiO_4$.[19] In spite of this, the electronic conductivity of $Li_x MSiO_4$ is supposed to be enhanced during delithiation process. Based on the analysis above, the variation of magnetic interaction among M ions also depends on the x in $Li_x MSiO_4$ due to the structural variation. In fully lithiated Li_2MSiO_4, the structural ordering as well as a larger $M-M$ interatomic distance strengthens the FM superexchange among M ions though O atoms. But in delithiated $LiMSiO_4$ and $MSiO_4$, the disordering $M-O$ polyhedra as well as short $M-M$ interatomic distances make the AFM directly exchange to be possible. However, the magnetic interaction is still a complicated issue.

Average Deintercalation Voltages. Following the well-established methods[34,35] and referring to the treatment approach in ref 19, the average deintercalation/intercalation voltage is given by

$$\bar{V} = -\frac{\Delta G}{\Delta x} \tag{3}$$

where Δx refers to the number of lithium transferred and ΔG is the Gibbs free energy differences between two intercalation limits. Because the effects due to changes in volume and entropy are small, the Gibbs energy difference can be approximated by the internal energy difference at 0 K (ΔE). This approximation has been further verified by the first-principles calculation, which indicated that the difference between ΔE at 0 K and at 300 K is only ~30 meV.[36] Under this approximation, the average voltage for Li deintercalation from a host material is given by

$$\bar{V} = -\frac{E[Li_{x_2}MSiO_4] - E[Li_{x_1}MSiO_4] - (x_2 - x_1)E[Li]}{x_2 - x_1} \tag{4}$$

Here, x_2 and x_1 are the Li composition before and after the lithium extraction in the host, that is, two group choices ($x_2 = 2$, $x_1 = 1$) for M^{2+}/M^{3+} and ($x_2 = 1$, $x_1 = 0$) for M^{3+}/M^{4+}, respectively. Hence, to determine an average deintercalation voltage, the cohesive energy of three compounds (Li_2MSiO_4, $LiMSiO_4$, $MSiO_4$) and Li metal were calculated by the GGA+U method within the VASP package. The cohesive energy of metallic Li was calculated in the *bcc* structure, which corresponds to the structural phase of the Li anode.

Figure 7 presents the calculated average voltages for both M^{2+}/M^{3+} and M^{3+}/M^{4+} reactions in the Li_2MSiO_4 (M = Mn, Fe, and Co) system, comparing with previous results corresponding to $Pmn2_1$ symmetry. Lithium deinsertion from Li_2FeSiO_4 will proceed in marked two step-voltage plateaus: a first at 3.28 V and a second at 4.64 V. Our results are slightly larger than experimental ones,[13] which may be induced by the tiny distinction between our optimized and experimental structures. The voltage step of 1.36 V at the composition $LiFeSiO_4$ is nested in the fact that one moves from a d^6 ion (Fe^{2+}) to a closed-shell d^5 ion (Fe^{3+}), which requires a small ionization energy as compared to the other M^{2+} to M^{3+} oxidations. However, the voltage step of 1.36 V is less than 1.6 V under the $Pmn2_1$ symmetry,[15] which further indicates that the reversibility and the cycling performance are improved in $P2_1$ Li_2FeSiO_4. In addition, Li et al.[37] and Guo et al.[38] also reported the voltages of Li_2FeSiO_4, 1.5 V at the first step and 4.8 V at the second step. In Li_2MnSiO_4 and Li_2CoSiO_4, the two voltage plateaus get closer, first at 4.02 V and second at 4.22 V for Mn case and first at 4.13 V and second at 4.87 V for Co case. This result on Mn system is in good agreement with the previous calculation value of 4.08 V for $P2_1/n$ Li_2MnSiO_4 by Arroyo-deDompablo et al.,[17] and also, the second cycle voltage is close to some experimental result.[39,40] But the first cycle voltage for Mn compound is much larger than experimental value of 1.5 V.[39,40] Comparing with the $Pmn2_1$ structure, at the first step, the average voltage of Fe compound is somewhat higher than previous experimental and theoretical results.[1,15] At the second step, in particular, the average voltages of Mn and Co compounds are noticeably lower than previous calculation results within the $Pmn2_1$ symmetry. As a result, with the $P2_1$ symmetry, the average voltages of Fe compound becomes high, while the voltages of the isostructural Mn and Co compounds are lowered to avoid the disadvantage of the voltage beyond reach in practice.[15] Furthermore, the band gaps of $P2_1$ structures are somewhat lower than those of $Pmn2_1$ symmetry so that the high electronic conductivity is obtained. Thus, $P2_1$ structural Li_2MSiO_4 (M = Mn, Fe, and Co) can be promising candidates as Li-ion battery materials due to these advantages of high electronic conductivity, suitable voltage, and advanced cycling performance.

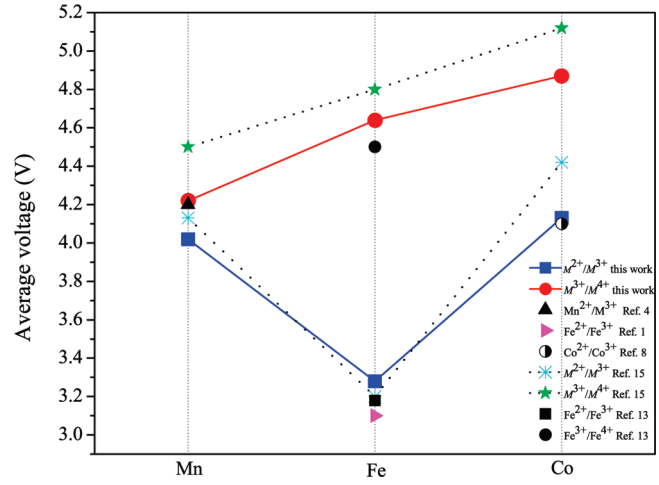

Figure 7. Average voltages for Li extractions from Li_2MSiO_4 (M = Mn, Fe, and Co). Available experimental and previous theoretical values are also shown: expt 1, ref 4; expt 2, ref 1; expt 3, ref 8; and calc 1, ref 15.

Conclusions

In summary, the $P2_1$ symmetrical Li_2MSiO_4 (M = Mn, Fe, and Co) has been studied by the first-principles calculation. The

exchange-correlation energy treated by GGA+U gives reasonable results. The delithiated LiMSiO$_4$ is a stable phase. However, the crystal structural transition results in the existence of M^{4+} five-coordination in MSiO$_4$, which make the stability of MSiO$_4$ increase. With the higher formation energies than those found in the $Pmn2_1$ situation, the stability of the intermediate phase LiMSiO$_4$ is decreasing. As a result, the reversibility and the cycling performance are improved in these $P2_1$ materials. During the process of lithium extraction, the transition metal ions are in high-spin state from M^{2+} to M^{3+} and to M^{4+}. The covalent bonding character is kept between Si and O atoms, with the σ bonding by the sp^3 hybridization. On the contrary, the ionic feature of $M-$O becomes more significant during the extraction of lithium. All these systems are semiconductors with the decrease of band gap during the Li extraction due to the charge transfer. In addition, the $M^{2+}-M^{2+}$ magnetic interaction is FM, while both $M^{3+}-M^{3+}$ and $M^{4+}-M^{4+}$ are AFM interactions mediated by O atoms. Within the $P2_1$ symmetry, the band gaps of Li_2MnSiO_4 and Li_2CoSiO_4 are lower, which results in the increase of electronic conductivity, and the second voltages of less than 5.0 V are more available, and low band gap Li_2FeSiO_4 has the slightly high voltage. It is an implication that the $P2_1$ symmetrical Li_2MSiO_4 (M = Mn, Fe, and Co) is a more promising Li-ion material.

Acknowledgment. The authors acknowledge the financial support of Grant No. HKRGC N−HKU705/07. Calculations were performed at the HPC Lab, Shenzhen Institute of Advanced Technology, CAS, P. R. China.

Supporting Information Available: Relaxed internal coordinates of all systems. This material is available free of charge via the Internet at http://pubs.acs.org.

References and Notes

(1) Nytén, A.; Abouimrane, A.; Armand, M.; Gustafsson, T.; Thomas, J. O. *Electrochem. Commun.* **2005**, *7*, 156.
(2) Nytén, A.; Kamali, S.; Häggström, L.; Gustafsson, T.; Thmas, J. O. *J. Mater. Chem.* **2006**, *16*, 2266.
(3) Nytén, A.; Stjerndahl, M.; Rensmo, H.; Siegbahn, H.; Armand, M.; Gustafsson, T.; Edström, K.; Thmas, J. O. *J. Mater. Chem.* **2006**, *16*, 3483.
(4) Dominko, R.; Bele, M.; Gaberšček, M.; Meden, A.; Remškar, M.; Jamnik, J. *Electrochem. Commun.* **2006**, *8*, 217.
(5) Gong, Z. L.; Li, Y. X.; Yang, Y. *Electrochem. Solid State Lett.* **2006**, *9*, A542.
(6) Zaghib, K.; Salah, A. A.; Ravet, N.; Mauger, A.; Gendron, F.; Julien, C. *J. Power Sources* **2006**, *160*, 1381.
(7) Dominko, R.; Bele, M.; Kokalj, A.; Gaberšček, M.; Jamnik, J. *J. Power Sources* **2007**, *174*, 457.
(8) Gong, Z. L.; Li, Y. X.; Yang, Y. *J. Power Sources* **2007**, *174*, 524.
(9) Li, Y. X.; Gong, Z. L.; Yang, Y. *J. Power Sources* **2007**, *174*, 528.
(10) Politaev, V. V.; Petrenko, A. A.; Nalbandyan, V. B.; Medvedev, B. S.; Shvetsova, E. S. *J. Solid State Chem.* **2007**, *180*, 1045.
(11) Dominko, R.; Conte, D. E.; Hanzel, D.; Gaberšček, M.; Jamnik, J. *J. Power Sources* **2008**, *178*, 842.
(12) Dominko, R. *J. Power Sources* **2008**, *184*, 462.
(13) Nishimura, S.; Hayase, S.; Kanno, R.; Yashima, M.; Nakayama, N.; Yamada, A. *J. Am. Chem. Soc.* **2008**, *130*, 13212.
(14) Larsson, P.; Ahuja, R.; Nytén, A.; Thomas, T. O. *Electrochem. Commun.* **2006**, *8*, 797.
(15) Arroyo-de Dompablo, M. E.; Armand, M.; Tarascon, J. M.; Amador, U. *Electrochem. Commun.* **2006**, *8*, 1292.
(16) Wu, S. Q.; Zhang, J. H.; Zhu, Z. Z.; Yang, Y. *Curr. Appl. Phys.* **2007**, *7*, 611.
(17) Arroyo-de Dompablo, M. E.; Dominko, R.; Gallardo-Amores, G. M.; Dupont, L.; Mali, G.; Ehrenberg, H.; Jamnik, J.; Morán, E. *Chem. Mater.* **2008**, *20*, 5574.
(18) Arroyo-de Dompablo, M. E.; Gallardo-Amores, J. M.; García-Martínez, J.; Morán, E.; Tarascon, J.-M.; Armand, M. *Solid State Ionics* **2008**, *179*, 1758.
(19) Wu, S. Q.; Zhu, Z. Z.; Yang, Y.; Hou, Z. F. *Comput. Mater. Sci.* **2009**, *44*, 1243.
(20) Kresse, G.; Furthmüller, J. *Comput. Mater. Sci.* **1996**, *6*, 5.
(21) Kresse, G.; Furthmüller, J. *Phys. Rev. B* **1996**, *54*, 11169.
(22) Blöchl, P. E. *Phys. Rev. B* **1994**, *50*, 17953.
(23) Madsen, G. K. H.; Blaha, P.; Schwarz, K.; Sjöstedt, E.; Nordström, L. *Phys. Rev. B* **2001**, *64*, 195134.
(24) Schwarz, K.; Blaha, P.; Madsen, G. K. H. *Comput. Phys. Commun.* **2002**, *147*, 71.
(25) Blaha, P.; Schwarz, K.; Madsen, G. K. H.; Kvasnicka, D.; Luitz, J. *WIEN2k: An Augmented Plane WaveLocal Orbitals Program for Calculating Crystal Properties*; Technische Universität: Wien, Austria, 2001.
(26) Monkhorst, H. J.; Pack, J. P. *Phys. Rev. B* **1976**, *13*, 5188.
(27) Perdew, J. P.; Burke, K.; Ernzerhof, M. *Phys. Rev. Lett.* **1996**, *77*, 3865.
(28) Anisimov, V. I.; Zaanen, J.; Andersen, O. K. *Phys. Rev. B* **1991**, *44*, 943.
(29) Dudarev, S. L.; Botton, G. A.; Savrasov, S. Y.; Humphreys, C. J.; Sutton, A. P. *Phys. Rev. B* **1998**, *57*, 1505.
(30) Jiang, X. F.; Guo, G. Y. *Phys. Rev. B* **2004**, *69*, 155108.
(31) Zhou, F.; Cococcioni, M.; Marianetti, C. A.; Morgan, D.; Ceder, G. *Phys. Rev. B* **2004**, *70*, 235121.
(32) http://www.webelements.com.
(33) Belharouak, I.; Abouimrane, A.; Amine, K. *J. Phys. Chem. C* **2009**, *113*, 20733.
(34) Courtney, I. A.; Tse, J. S.; Mao, O.; Hafner, J.; Dahn, J. R. *Phys. Rev. B* **1998**, *58*, 15583.
(35) Aydinol, M. K.; Kohan, A. F.; Ceder, G.; Cho, K.; Joannopoulos, J. *Phys. Rev. B* **1997**, *56*, 1354.
(36) Deiss, E.; Wokaun, A.; Barras, J. L.; Daul, C.; Dufek, P. *J. Electrochem. Soc.* **1997**, *144*, 3877.
(37) Li, L.-M.; Guo, H.-J.; Li, X.-H.; Wang, Z.-X.; Peng, W.-J.; Xiang, K.-X.; Cao, X. *J. Power Sources* **2009**, *189*, 45.
(38) Guo, H.-J.; Xiang, K.-X.; Cao, X.; Li, X.-H.; Wang, Z.-X.; Li, L.-M. *Trans. Nonferrous Met. Soc. China* **2009**, *19*, 166.
(39) Liu, W.; Xu, Y.; Yang, R. *J. Alloys Compd.* **2009**, *480*, L1.
(40) Ghosh, P.; Mahanty, S.; Basu, R. N. *J. Electrochem. Soc.* **2009**, *156* (8), A677.

JP910746K

Supporting Information

Structural, electronic, and electrochemical properties of cathode materials Li_2MSiO_4 (M = Mn, Fe, and Co): Density functional calculations

Guohua Zhong[†], Yanling Li[‡], Peng Yan[¶], Zhuang Liu[†], Maohai Xie[§], and Haiqing Lin[*,†]

[†]*Center for Photovoltaics Solar Cell, Shenzhen Institutes of Advance Integration Technology,Chinese Academy of Sciences, Shenzhen, 518055, P. R. China*

[‡]*Department of Physics, Xuzhou Normal University, Xuzhou, 221116, P. R. China*

[¶]*Department of Physics, Binzhou Medical University, Yantai, 264003, P. R. China*

[§]*Department of Physics, The University of Hong Kong, Pokfulam Road, Hong Kong, P. R. China*

Table *S1* Relaxed internal coordinates in Li_2MSiO_4 (*M* = Mn, Fe, and Co).

	M = Mn			*M* = Fe			*M* = Co		
	x	*y*	*z*	*x*	*y*	*z*	*x*	*y*	*z*
Li1	0.66576	0.92558	0.66212	0.66414	0.92366	0.66561	0.66653	0.92532	0.66219
Li2	0.16550	0.80701	0.16279	0.16354	0.80879	0.33365	0.16603	0.80751	0.16287
Li3	0.57943	0.40841	0.08363	0.57651	0.40656	0.08339	0.57777	0.41387	0.08340
Li4	0.07986	0.32183	0.58371	0.07686	0.32427	0.58342	0.07796	0.31758	0.58358
*M*1	0.29639	0.91803	0.54574	0.29254	0.92016	0.54182	0.29934	0.92357	0.54813
*M*2	0.79608	0.81237	0.04574	0.79200	0.81113	0.04164	0.79895	0.80740	0.04801
Si1	0.03584	0.80516	0.78729	0.04281	0.80907	0.79385	0.03937	0.80543	0.79033
Si2	0.53674	0.92556	0.28762	0.54332	0.92142	0.29413	0.53981	0.92548	0.29045
O1	0.85814	0.91228	0.82583	0.86198	0.91235	0.83158	0.85680	0.90992	0.83006
O2	0.35818	0.81623	0.32715	0.36176	0.81625	0.33281	0.35661	0.81936	0.33114
O3	0.43165	0.30991	0.89115	0.42671	0.30441	0.88623	0.42945	0.31173	0.89206
O4	0.93236	0.42085	0.39049	0.92704	0.42676	0.38554	0.92961	0.41907	0.39152
O5	0.68164	0.82803	0.43188	0.68939	0.82561	0.44169	0.68364	0.82226	0.43368
O6	0.18074	0.90417	0.93191	0.18875	0.90664	0.94171	0.18321	0.91018	0.93374
O7	0.96637	0.98102	0.21728	0.96027	0.98588	0.21377	0.96030	0.97882	0.21190
O8	0.46657	0.75143	0.71744	0.46093	0.74669	0.71378	0.46074	0.75321	0.71194

Table *S2* Atomic coordinates of stable $LiMSiO_4$ (*M* = Mn, Fe, and Co).

	M = Mn			*M* = Fe			*M* = Co		
	x	*y*	*z*	*x*	*y*	*z*	*x*	*y*	*z*
Li1	0.58506	0.40554	0.07034	0.58862	0.42047	0.08470	0.58061	0.42439	0.08560
Li2	0.08574	0.32630	0.56916	0.08872	0.31158	0.58456	0.08074	0.30763	0.58539
*M*1	0.29252	0.93810	0.51945	0.30143	0.92253	0.52885	0.29933	0.92775	0.53150
*M*2	0.79189	0.79330	0.01874	0.80135	0.80943	0.02864	0.79918	0.80418	0.03138
Si1	0.08224	0.80888	0.80965	0.05800	0.80776	0.78117	0.06096	0.80504	0.78918
Si2	0.58261	0.92282	0.31007	0.55805	0.92415	0.28314	0.56114	0.92666	0.28930
O1	0.90911	0.85745	0.84060	0.88039	0.87078	0.82033	0.88029	0.86898	0.83152
O2	0.40978	0.87262	0.34157	0.38043	0.86119	0.32054	0.38044	0.86271	0.33165
O3	0.40368	0.30361	0.89839	0.41644	0.33636	0.91926	0.41740	0.33282	0.90881
O4	0.90399	0.42851	0.39842	0.91642	0.39561	0.41925	0.91748	0.39977	0.40866
O5	0.70454	0.79010	0.46469	0.68124	0.76846	0.41168	0.68837	0.77828	0.42137

O6	0.20370	0.94234	0.96507	0.18108	0.96365	0.91163	0.18821	0.95380	0.92122
O7	0.88568	0.01142	0.19826	0.90799	0.00156	0.20296	0.90951	0.99589	0.20326
O8	0.38568	0.72071	0.69919	0.40806	0.73051	0.70299	0.40975	0.73637	0.70333

Table *S3* Atomic coordinates in MSiO$_4$ (M = Mn, Fe, and Co).

	M = Mn			M = Fe			M = Co		
	x	*y*	*z*	*x*	*y*	*z*	*x*	*y*	*z*
*M*1	0.19863	0.82549	0.50838	0.20918	0.82005	0.51442	0.21342	0.81400	0.51338
*M*2	0.72505	0.72811	0.02386	0.72601	0.72947	0.02342	0.72855	0.73047	0.02392
Si1	0.05420	0.78942	0.82667	0.05446	0.78909	0.82816	0.05817	0.79028	0.82991
Si2	0.53030	0.90280	0.31000	0.54338	0.89389	0.31633	0.54290	0.90453	0.32105
O1	0.85343	0.83175	0.88330	0.85135	0.83396	0.88035	0.82416	0.84373	0.86507
O2	0.31384	0.86545	0.35149	0.32322	0.85601	0.35763	0.31995	0.87043	0.36480
O3	0.49607	0.49176	0.86445	0.49175	0.49601	0.86424	0.49552	0.50013	0.86771
O4	0.99754	0.50346	0.37174	0.99281	0.50884	0.36929	0.99841	0.50896	0.37018
O5	0.69550	0.80107	0.42887	0.69307	0.79368	0.42795	0.69849	0.80194	0.42781
O6	0.24820	0.04544	0.90512	0.24846	0.05275	0.90564	0.24885	0.05994	0.90168
O7	0.88210	0.00117	0.18198	0.87745	0.01345	0.17822	0.89447	0.02931	0.16481
O8	0.38864	0.72801	0.63153	0.39200	0.70797	0.62981	0.39410	0.71852	0.64427